Facile synthesis of Cu-LDH with different Cu/Al molar ratios: application as antibacterial inhibitors

Hadja Alia Tabti[1] · Mehdi Adjdir[2,3] · Abdelkader Ammam[4] · Baghdad Mdjahed[5] · Brahim Guezzen[5] · Amina Ramdani[6] · Choukry Kamel Benddedouche[7] · Noria Bouchikhi[1] · Nadir Chami[8]

Abstract

A range of Cu-LDHs has been synthesized by co-precipitation using metal nitrate precursors and sodium carbonate under varying molar ratios Cu/Al ($Cu_{0.05}$–$Al_{0.15}$, $Cu_{0.10}$–$Al_{0.10}$, $Cu_{0.14}$–$Al_{0.06}$, and $Cu_{0.15}$–$Al_{0.05}$). The uncalcined and calcined Cu-LDHs were characterized by powder X-ray diffraction and N_2 adsorption–desorption. The uncalcined solids showed clear hydrotalcite-like crystalline phases having a particle measurement between 5 and 16 nm. The best structure is attributed to the sample $Cu_{0.05}$–$Al_{0.15}$-LDHs. The particular surface areas are ranging between 40 and 92 m^2/g, while the calcined samples showed the formation of Cu and Mg oxides. The antibacterial activity of Cu-LDHs with various molar ratios Cu/Al and their calcined phases were estimated towards multiple types of bacteria (*Escherichia coli*, *Pseudomonas aeruginosa*, *Enterococcus faecalis*, *Staphylococcus aureus*, and *Bacillus Subtilis*). The $Cu_{0.10}$–$Al_{0.10}$-LDHs sample shows high activity against all types of bacteria either for calcined or uncalcined materials. The obtained results of the application of Cu-LDHs antibacterial inhibitors seem to be quite promising material in the antibacterial fields.

Keywords LDHs · Calcination · Copper · XRD · N_2-sorption · Size · Antibacterial inhibition

✉ Hadja Alia Tabti
hadjaalia.tabti@gmail.com

✉ Mehdi Adjdir
mehdi.adjdir@daad-alumni.de

Extended author information available on the last page of the article

Introduction

Layered double hydroxides (LDHs) are known as anionic clays or hydrotalcite based on the structure of Brucite charged positively ($Mg(OH)_2$). LDHs can be described by the general formula: $[M^{2+}\ M^{3+}(OH)_2]^{x+}[A^{n-}_{x/y}{\cdot}y{\cdot}H_2O]^{x-}$ where, M^{2+} denotes bivalent cations as (Cu^{2+}, Mg^{2+}, Zn^{2+}) and M^{3+} as trivalent cations (Al^{3+}, Fe^{3+}, Cr^{3+}. ect). Both bivalent and trivalent cations occupy octahedral coordination with six OH groups. The principal interest of the layered double hydroxide lies in the possibility of modifies the layers by insertion or substitution of divalent and trivalent cations. Layered double hydroxides can contain different types of divalent and trivalent cations like magnesium; aluminium; zinc, nickel [1], cobalt [2], chrome; iron, and gallium ions [3] except for copper. The incompatibility of copper in the octahedral networks of the hydrotalcite-like phase is explained to the effect distortion of Jahn–Teller. In this case, various works have been published for the synthesis of LDHs with copper. Yamoka et al. [4] reviewed the synthesis of LDHs with different molar ratios of Cu/Al; the layered double hydroxide obtained has a layered structure that is included in the monoclinic system. Alejandre et al. [5] observed the coexistence of other phases such as gibbsite with Cu–Al-LDHs, synthesized under various molar ratios Cu/Al. Fogg et al. [6] found that Cu–Al-LDHs with molar ratio Cu/Al = 0.25 leads to orthorhombic symmetry. Carja et al. [7] reported the study of the influence of substitution of magnesium with copper and iron on the texture of Cu–Al-LDHs; they discovered that when copper substituted with magnesium in the layered double hydroxide, the compound showed a mesoporous characteristic with an increase in the size of mesopores. From synthesis methodologies, several methods have been developed for the preparation of LDHs. Kuang et al. [8] examined the combination of the different techniques of LDHs synthesis and its influence on the structure and morphology of the resulting LDHs. Among these synthesis methods, the co-precipitation method [9, 10], urea process, the hydrothermal method [11, 12], and microwave method [12, 13]. Concerning their application in fields, LDHs with transition metals have acquired a lot of interest; in particular copper and iron [14, 15]. Carja et al. [7], Kim et al. [16] and Zhang et al. [17] used the Cu-LDHs and its calcined materials in different applications as catalytic reaction [15], photocatalytic activity [18], photodegradation of dyes [19, 20], and as antibacterial inhibitors. Copper has antibacterial property and is a natural antibacterial agent; not only in its natural state, but also as nanoparticles [21, 22], and as copper oxide [23–25]. Mishra et al. [26] reported the application of Cu-substituted-Zn-LDHs and its calcined materials as an antibacterial inhibitor against both gram-positive (*S. aureus)* and gram-negative (*E. coli*) bacteria. They perceived that the calcined materials show better antibacterial activity than uncalcined ones.

This work aimed to the optimization of the molar ratio Cu/Al ($Cu_{0.05}$–$Al_{0.15}$, $Cu_{0.10}$–$Al_{0.10}$, $Cu_{0.14}$–$Al_{0.06}$, and $Cu_{0.15}$–$Al_{0.05}$) in the synthesis of the Mg–Cu–Al–CO_3 using the co-precipitation method; the effect of the calcination on the formation of new crystalline metal oxide phases and ultimately the application of either the uncalcined or calcined Mg–Cu–Al-LDHs as antibacterial inhibitors experimental.

Experimental

Method

The Mg–Cu–Al–CO_3 LDHs samples with different molar ratios Cu/Al ($Cu_{0.05}$–$Al_{0.15}$, $Cu_{0.10}$–$Al_{0.10}$, $Cu_{0.14}$–$Al_{0.06}$, and $Cu_{0.15}$–$Al_{0.05}$) were prepared successfully using the co-precipitation method. Table 1 showed the various molar ratios between Mg^{2+}, Cu^{2+} and Al^{3+}.

In a general synthesis, the samples were obtained together by adding dropwise, at room temperature, a solution containing Mg $(SO_4)\cdot 1H_2O$, $Cu(NO_3)\cdot 3H_2O$, and $Al(NO_3)_3\cdot 9H_2O$ with different molar ratios Cu/Al and a suspension of NaOH (1 M) to a vigorously stirred solution (45 ml) containing Na_2CO_3 (0.42 M) until managing the pH 10. The suspension obtained (blue precipitate) was automatically stirred for a further 24 h at 80 °C under reflux to form Mg–Cu–Al–CO_3. The precipitate formed was separated by centrifugation and washed several times with distilled water to eliminate excess soluble ions, until the pH of the filtrate was 7. The four precipitates obtained with different molar ratios Cu/Al were dried in an oven at 75 °C overnight. The calcination of the various samples obtained was carried out in an oven under air for 6 h at a temperature of 450 °C.

Antibacterial activity

The antibacterial activity of Mg–Cu–Al–CO_3 synthesized with several molar ratios Cu/Al and their calcined phases were evaluated towards different types of bacteria (*Escherichia coli*, *Pseudomonas aeruginosa, Enterococcus faecalis*, *Staphylococcus aureus*, and *Bacillus subtilis*) using the very method presented by Zahraoui et al. [27]. 0.5 ml of cultures were diluted in 20 ml of Muller Hinton liquid. The latter, apparently solid, is melted by heating and then cooled before putting in contact with the microbial suspension. The mixture was placed in Petri dishes of 90 mm. Using a Pasteur pipette, wells of 7 mm diameter are dug in Muller Hinton agar poured into sterile Petri plates. The same measure (20 mg) of each sample of Mg–Cu–Al–CO_3 synthesized with different molar ratios and its calcined form was put in the wells. Ensuing, the antibacterial activity is determined after incubation of the dishes in an oven at 37 °C for 24 h. The inhibition zone around the spots was observed visually.

Table 1 Different molar ratios between Mg^{2+}, $Cu^{2+}$and Al^{3+}

Samples	Mg^{2+}/Al^{3+}	$(Mg^{2+}+Cu^{2+})/Al^{3+}$	Molar concentration (mol/l)		
			$Mg(SO_4)\cdot 1H_2O$	$Cu(NO3)_2\cdot 3H_2O$	$Al(NO3)_3\cdot 9H_2O$
$Cu_{0.05}$–$Al_{0.15}$	5.33	5.67	0.72	0.045	0.135
$Cu_{0.10}$–$Al_{0.10}$	8	9	0.72	0.090	0.090
$Cu_{0.14}$–$Al_{0.06}$	13.33	15.67	0.72	0.126	0.053
$Cu_{0.15}$–$Al_{0.05}$	16	19	0.72	0.132	0.045

Characterization

XRD patterns were recorded for all the samples in order to check the formation and structure of Mg–Cu–Al-LDHs. The diffraction patterns were recorded in the 2θ range of 1°–80° with a step size of 0.02° and a step time of 5 s on a Bruker D5000 diffractometer with CuKα (λ = 0.15406 nm) radiation equipped with a graphite monochromator and scintillation counter. A CuKα anode was powered with 40 kV and 40 mA. N_2-sorption measurements were performed at 77 K using a Quantachrome Autosorb 1MP. The samples were degassed at 383 K in vacuum for 24 h before measurements. Specific surface areas were calculated by using the Brunauer–Emmett–Teller (BET) method [28].

Results and discussion

X-ray diffractions

Figure 1. shows the X-ray diffraction of Mg–Cu–Al-LDHs prepared with different Cu/Al molar ratios ($Cu_{0.05}$–$Al_{0.15}$, $Cu_{0.10}$–$Al_{0.10}$, $Cu_{0.14}$–$Al_{0.06}$, and $Cu_{0.15}$–$Al_{0.05}$). Diffractograms of all uncalcined samples revealed the presence of a crystalline phase similar to the hydrotalcite-like type in all samples, it attributed to the rhomboedral structure [29]. The corresponding XRD patterns exhibited the main peaks characteristic of layered hydrotalcite phase at diffraction angles $2\theta = 11.31$; 23; 35.2 and 61.1°, which correspond to the planes (003), (006), (009) and (110), respectively. No impurity peak can be observed and no crystalline phase of oxide peaks was detected, which indicated that the user process in this work gives a pure phase of layered double hydroxide [30]. But while the pure phase of LDHs was obtained, the crystallinity of the obtained materials is low. We noticed that the reflections (003), (006), and (009) which characterize the lamellar phase of LDHs is not observed in the case of Mg–Cu–CO_3. This absence is attributed to the Jahn–Teller effect of the

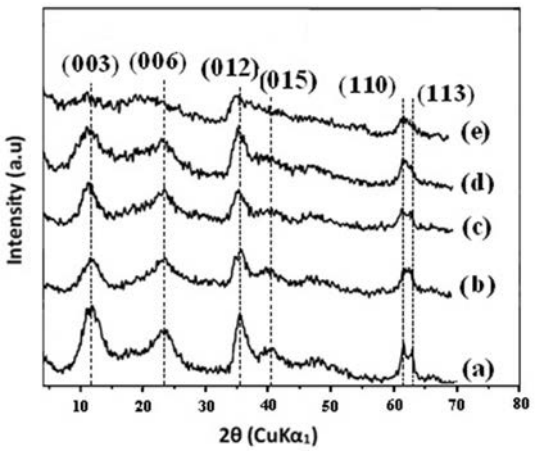

Fig. 1 XRD patterns of Mg–Cu–Al-LDHs synthesized with different Cu/Al molar ratios (a = $Cu_{0.05}$–$Al_{0.15}$, b = $Cu_{0.10}$–$Al_{0.10}$, c = $Cu_{0.14}$–$Al_{0.06}$, d = $Cu_{0.15}$–$Al_{0.05}$, and e = Mg–Cu–CO_3)

copper ions. The latter causes a distortion of the ordered octahedron to square plane D4h, either by compressing the axial bonds or by lengthening them.

Powder X-ray diffraction patterns of Mg–Cu–Al–CO_3 samples calcined at 450 °C are shown in Fig. 2. With calcination at 450 °C; the initial structure of layered double hydroxide was progressively destroyed, the peaks characteristic of the hydrotalcite structure disappear and are replaced by those attributable to CuO, MgO. The diffraction patterns showed the formation of Cu, Mg oxides phases, which are justified by the appearance of large peaks of CuO and MgO. They are characterized by the reflections of the peaks (200) at $2\theta = 37°–43°$ and (220) at $2\theta = 62°$. The formation of Al_2O_3 is not detected by X-ray diffraction; they are generally in the amorphous state, this may be due to the localization of Al^{3+} cation on the tetrahedral sites after calcination. These transformation can be explained by the dehydroxylation followed by the elimination of water molecules of the interlamellar domain and the decomposition of carbonate anions on the interlayered spacing [31, 32].

Table 2 showed the experimental parameters of Mg–Cu–Al–CO_3 samples; the basal spacing (d) was calculated using Bragg's law equation: $2d\sin\theta = n\lambda$, the size particle (D) was determined by Scherer equation: $\beta = k\lambda/D\cos\theta$. Where β is the full width at half maximum, (λ) is the wavelength of CuKα, (θ) is the angle of incidence and (k) the constant of Scherer, (a) corresponds to the average metal–metal distance within the layers, and (c) corresponds to three times the layer-to-layer distance

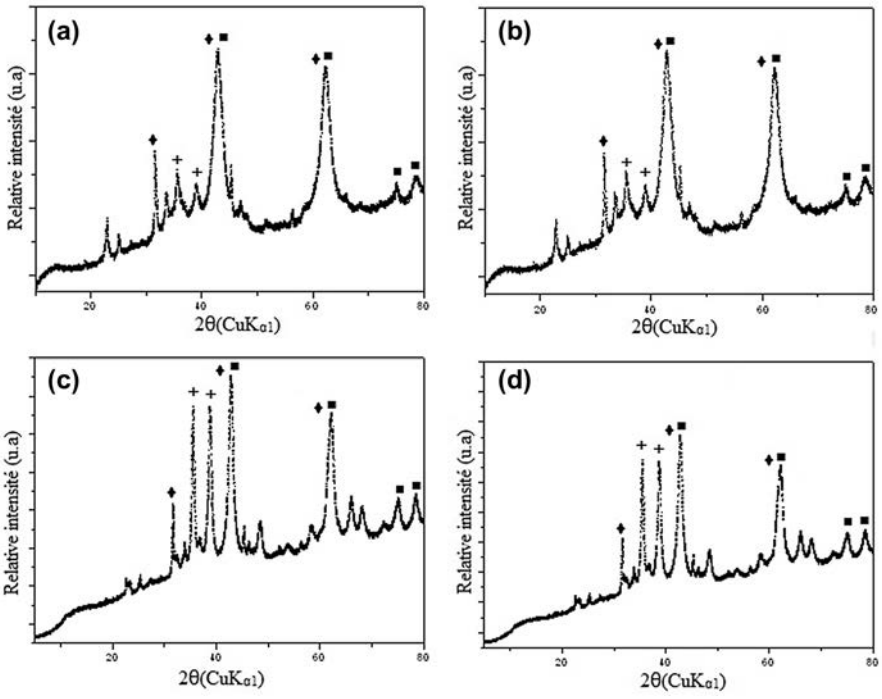

Fig. 2 XRD patterns of Mg–Cu–Al-LDHs samples calcined and synthesized with different Cu/Al molar ratios. ■: MgO; +: CuO (a = $Cu_{0.05}$–$Al_{0.15}$, b = $Cu_{0.10}$–$Al_{0.10}$, c = $Cu_{0.14}$–$Al_{0.06}$, and d = $Cu_{0.15}$–$Al_{0.05}$)

Table 2 Experimental parameters of the uncalcined samples

Samples	$2\theta_{(003)}$	a (Å)	c (Å)	$\beta_{(003)}$	$\beta_{(110)}$	S_{BET}	$D^{¤}_{(003)}$	$D^{¤}_{(110)}$
$Cu_{0.05}$–$Al_{0.15}$	11.31	3.14	23.49	0.306	0.191	92	26.08869	16.676176
$Cu_{0.10}$–$Al_{0.10}$	11.54	2.96	26.4	0.317	0.195	84	25.18846	16.554184
$Cu_{0.14}$–$Al_{0.06}$	10.62	2.66	27.21	0.322	0.204	51	24.77803	16.135946
$Cu_{0.15}$–$Al_{0.05}$	10.16	2.36	29.61	0.341	0.214	48	23.38890	15.859649

a, c, lattice cell parameters: ($c=3d_{003}$, $a=2d_{110}$); $D^{¤}$, particle sizes calculated using the Scherrer equation; β, full width at half maximum. S_{BET}, total surface area calculated by BET method

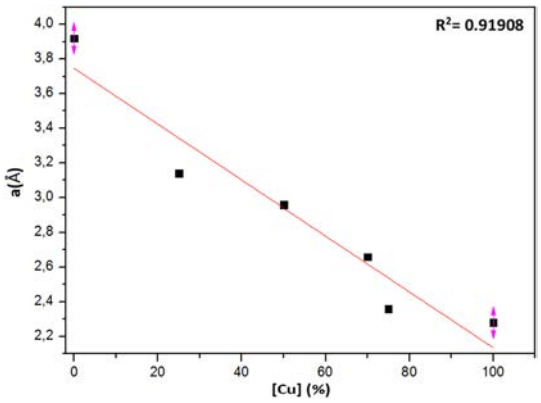

Fig. 3 Influence the copper content [Cu^{2+}] on the lattice parameter (a)

($c=3d_{003}$) [33]. According to the results of Table 2 and Fig. 3, the parameter (a) decreases when the copper content increases. These results can be attributed to the difference in cation-oxygen bond length between Cu–O (1.95 Å), Mg–O (2.106 Å) and Al–O which is equal to (1.735 Å) [34]. Also, this variation can be caused by the location of oxygen atoms either in the basal plane of the octahedral (an equatorial bond between the central cation and the four oxygen ions), or on the axis (z) which contains the two others oxygen existing at the top of the octahedron (axial bonds). This is a reasonable result because the copper ions have an ionic radius greater than magnesium and aluminium ions [Cu^{2+} (0.76 Å), Mg^{2+} (0.72 Å), and Al^{3+} (0.50 Å)].

It is known that the (c) parameter is influenced only by the intercalated anion in the interlamellar space. It didn't evolve by the substitution of cations in the layer of LDHs. Kim et al. [16] and Mishra et al. [26] reported the synthesis of Cu-substituted Zn–Al-LDHs with chloride (Cl^{-}) and carbonate (CO_3^{-2}) as an intercalated anion. They founded a small deviation in the values of (c) parameter. In our case, we used carbonate and nitrate as interlayered anions. Based on the results given in Table 2 and Fig. 4, we notice that, when Cu^{2+} content increases (c) parameter increases; it varies between 23.79 and 29.61 Å. These results may be due to the nature of the interlamellar anions as well as to the difference in the size, electronegativity, affinity, and orientation of these anions d^{-}_{NO} (8.76 Å) > d^{-2}_{CO} (7.56 Å).

The value of the full width at half maximum (FWHM) is very important in determining the crystallinity of the material; because when it decreases, the

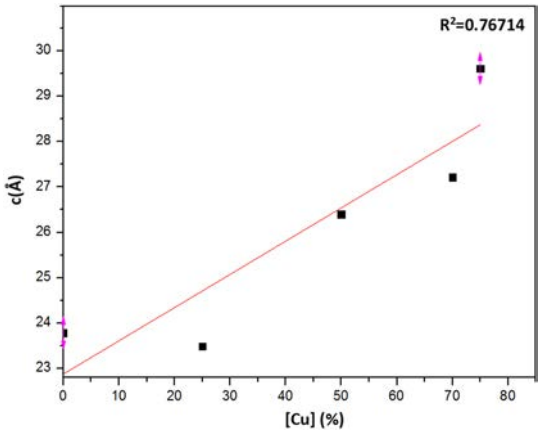

Fig. 4 Influence the copper content [Cu^{2+}] on the lattice parameter (*c*)

crystallinity of this material increases. According to the results obtained in Table 2 and Fig. 5, we noticed the increase of the full width at half maximum of the (110) and (003) diffraction peaks with the increase of copper content. Therefore, it is concluded that the crystallinity of Mg–Cu–Al–CO_3 synthesized is directly influenced by the copper and aluminium content. This is in agreement with the data reported by Johana Rodriguez Ruiz et al. [35] which showed that the Cu–Zn–Al–CO_3 materials synthesized with high copper content lead to the formation of copper hydroxide, due to the Jahn–Teller effect of copper ions. So, the increase in trivalent cations promotes the formation of the most stable hydrotalcite structure. In our case, we concluded that the best crystallinity attribute to the $Cu_{0.05}$–$Al_{0.15}$ ratio, and the minimum threshold for obtaining a layered double hydroxide with rhombohedra symmetry is $Cu_{0.15}$–$Al_{0.05}$ in agreement with the works of Britoo et al. [36] and Fogg et al. [6] who reported that the synthesis of Cu–Al-LDHs with ratio Cu/Al = 0.25 presents a rhombohedra symmetry.

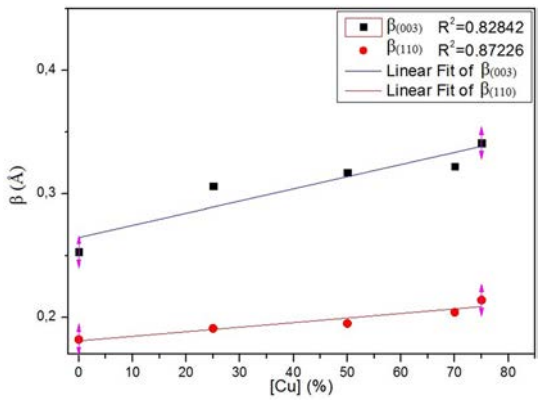

Fig. 5 Influence the copper content [Cu^{2+}] on the FWHM (β)

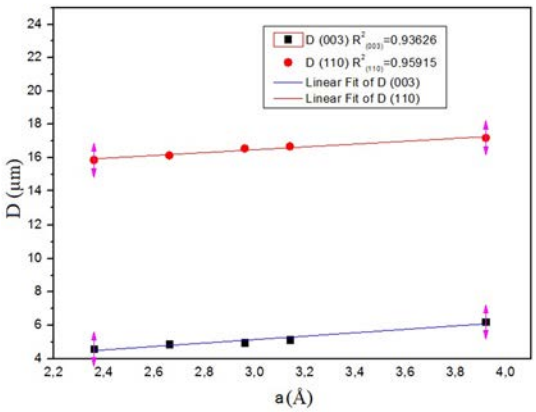

Fig. 6 Influence of copper content [Cu^{2+}] on particle size

In Fig. 6, we observed when the Cu^{2+} content increases, the size particle decreases, because of bond length between Cu–O which causes a vibration of the cell. So for the stabilization of the system, the particle will probably subdivide to smaller size compared to that found in the cases of Al–O. We noticed else, when the parameter (a) increases, the particle size increases. This means that the bond length between cation-oxygen-cation increases, this is verified in the case of the copper ion where the length Cu–O is approximately (1.95 Å) compared to those of Al–O and Mg–O which are equal at (1.73 Å) and (2.106 Å), respectively.

N_2 adsorption–desorption

Figure 7 shows the Nitrogen sorption isotherms for Mg–Cu–Al-LDHs synthesized with different Cu/Al molar ratios. The isotherm exhibited type II according to the IUPAC classification of the materials [28, 37]. This type isotherm characterizes a non-porous or macroporous solid ($\varphi > 100$ Å). The corresponding textural proprieties were shown in Table 2. All the synthesized Mg–Cu–Al-LDHs possessed no

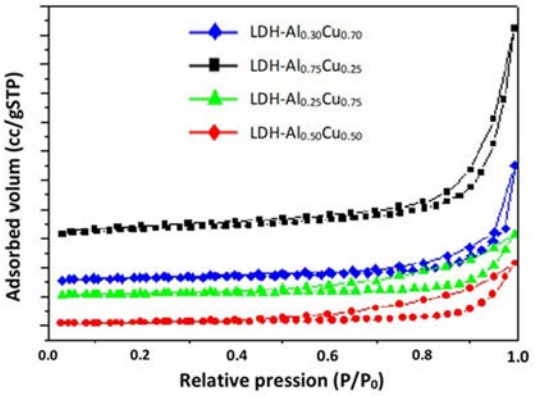

Fig. 7 Adsorption/desorption isotherms of Mg–Cu–Al-LDHs

micropores volumes. The position of the inflection point "β" in the low relative pressure range $P/P_0 < 0.1$, indicates a weak affinity of the adsorbate (N_2) and the adsorbent (LDHs) [37]. The hysteresis loop occurs during desorption [38]. Specific surface areas of the Mg–Cu–Al-LDHs determinate by the BET method. The calculated BET surface area of all the samples was 92, 84, 51, and 42 m^2/g for the samples synthesized with Cu/Al molar ratios ($Cu_{0.05}$–$Al_{0.15}$, $Cu_{0.10}$–$Al_{0.10}$, $Cu_{0.14}$–$Al_{0.06}$, and $Cu_{0.15}$–$Al_{0.05}$), respectively, as shown in Table 2.

The antibacterial activity of Mg–Cu–Al-LDHs

The antibacterial activity of Mg–Cu–Al-LDHs synthesized with different molar ratios Cu/Al ($Mg_{0.80}$–$Cu_{0.05}$–$Al_{0.15}$, $Mg_{0.80}$–$Cu_{0.10}$–$Al_{0.10}$, $Mg_{0.80}$–$Cu_{0.14}$–$Al_{0.06}$, and $Mg_{0.80}$–$Cu_{0.15}$–$Al_{0.05}$) and its different calcined products were carried out both gram-negative (*Escherichia coli*, *Pseudomonas aeruginosa)*, and gram-positive (*Staphylococcus aureus*, *Bacillus subtilis*, *Enterococcus faecalis)* bacteria. The inhibition zones are shown in Figs. 8 and 9. Also, Tables 3 and 4 display the measurements of inhibition zone of uncalcined and calcined samples, respectively. According to Mishra et al. [39, 40], layered double hydroxide has previously given negative results in the antibacterial test against Gram-positive and Gram-negative bacteria. The same results were obtained in the case of zeolites, magadiite [41], MCM-41 [42], and clays in their normal state without any

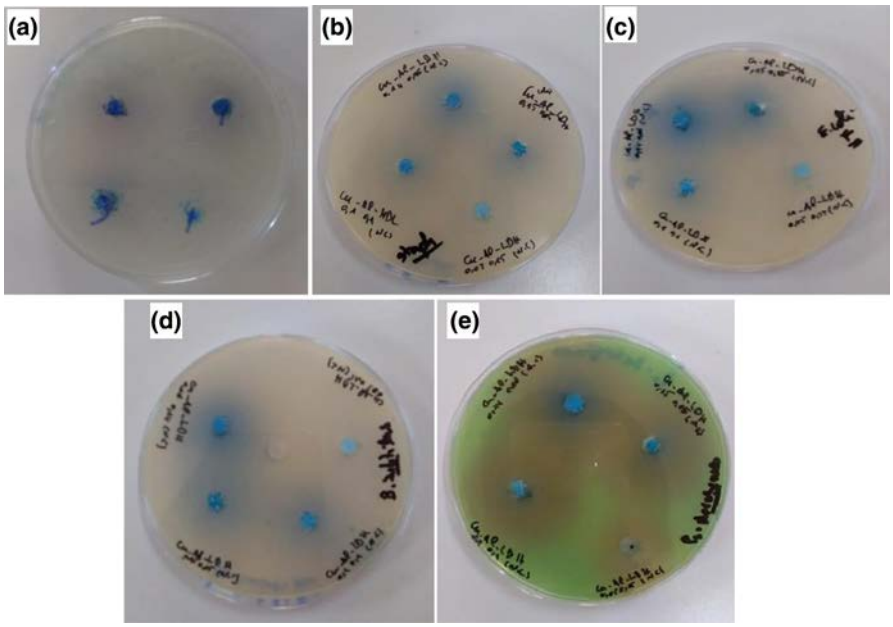

Fig. 8 Antibacterial test of Mg–Cu–Al-LDHs uncalcined materials synthesized with different molar ratios Cu/Al ($Mg_{0.80}$–$Cu_{0.05}$–$Al_{0.15}$, $Mg_{0.80}$–$Cu_{0.10}$–$Al_{0.10}$, $Mg_{0.80}$–$Cu_{0.14}$–$Al_{0.06}$, and $Mg_{0.80}$–$Cu_{0.15}$–$Al_{0.05}$) against (**a** *E. coli*, **b** *S. aureus*, **c** *E. faecalis*, **d** *B. Subtilis,* **e** *P. aeruginosa*) bacteria

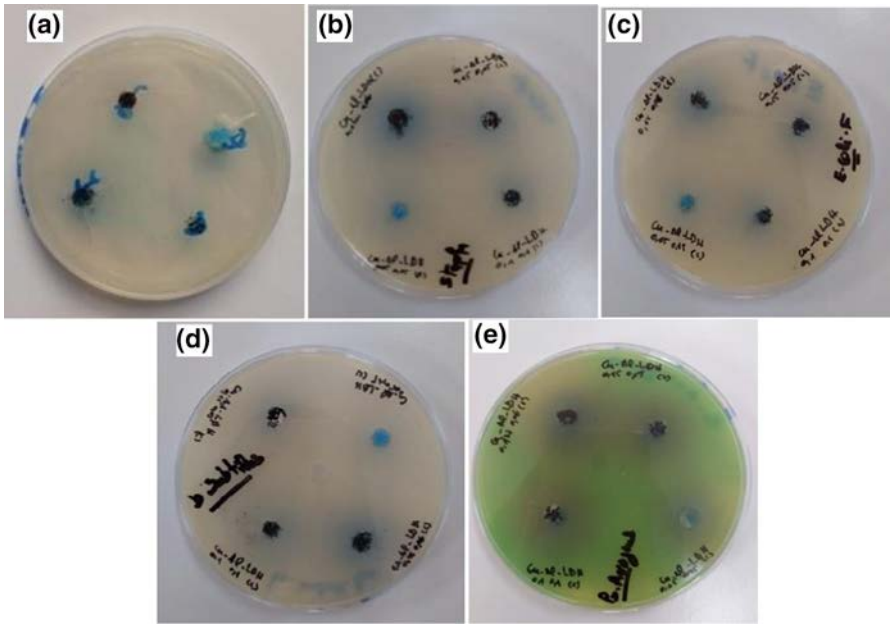

Fig. 9 Antibacterial test of Mg–Cu–Al-LDHs calcined materials and synthesized at different molar ratios Cu/Al ($Mg_{0.80}$–$Cu_{0.05}$–$Al_{0.15}$, $Mg_{0.80}$–$Cu_{0.10}$–$Al_{0.10}$, $Mg_{0.80}$–$Cu_{0.14}$–$Al_{0.06}$, and $Mg_{0.80}$–$Cu_{0.15}$–$Al_{0.05}$) against (**a** *E.Coli*, **b** *S. aureus*, **c** *E. faecalis*, **d** *B. Subtilis*, **e** *P. aeruginosa*,) bacteria

Table 3 Antibacterial test results of Mg–Cu–Al–CO_3 uncalcined materials synthesized with different molar ratios against the bacterial stain

Samples as-synthesized	Inhibition zone size (in mm)				
	E. coli (a)	*S. aureus* (b)	*E. faecalis* (c)	*B. Subtilis* (d)	*P. Aeruginosa* (e)
$Cu_{0.05}$–$Al_{0.15}$	00	00	00	00	22
$Cu_{0.10}$–$Al_{0.10}$	17	18	21	19	35
$Cu_{0.14}$–$Al_{0.06}$	13	22	28	22	32
$Cu_{0.15}$–$Al_{0.05}$	15	20	20	22	31

Table 4 Antibacterial test results of Mg–Cu–Al–CO_3 materials synthesized with different molar ratios and calcined at 450 °C against the bacterial stain

Samples calcined (450 °C)	Inhibition zone size (in mm)				
	E. coli (f)	*S. aureus* (g)	*E. faecalis* (h)	*B. Subtilis* (i)	*P. Aeruginosa* (j)
$Cu_{0.05}$–$Al_{0.15}$	19	15	17	12	23
$Cu_{0.10}$–$Al_{0.10}$	23	20	15	23	29
$Cu_{0.14}$–$Al_{0.06}$	15	24	17	22	30
$Cu_{0.15}$–$Al_{0.05}$	22	17	20	12	26

modification or incorporation of metals during their synthesis [43, 44]. However, Zahraoui et al. [27] reported the synthesis of Cu-magadiite with different counter ions of copper; the result materials applied as antibacterial agents, it gives great results against both grams positive and gram-negative bacteria.

In our study, all uncalcined samples of Mg–Cu–Al–CO_3 synthesized with different molar ratios presented good antibacterial activity with inhibition diameters varied between 15 and 28 mm against *Escherichia coli* Gram-negative bacteria, and *Staphylococcus aureus*, *Bacillus subtilis*, and *Enterococcus faecalis* Gram-positive bacteria; excepted for the $Mg_{0.80}$–$Cu_{0.05}$–$Al_{0.15}$–CO_3. For the *Pseudomonas aeruginosa* bacteria, we noticed that Mg–Cu–Al-LDHs synthesized with different Cu/Al molar ratios (calcined and uncalcined samples) presented important inhibition diameters compared to those obtained with the other bacteria also for the $Mg_{0.80}$–$Cu_{0.05}$–$Al_{0.15}$–CO_3 materials. For the calcined samples; calcination of materials at 450 °C show more effective antibacterial activity as compared to those uncalcined ones towards most of the bacteria studied with inhibition diameters varied between 12 and 30 nm, as revealed from Fig. 9 and Table 4. Compared to the results reported in the literature, we notice that the antibacterial activity of copper oxides obtained after the calcination of our material is more effective than that synthesized by Jadhav et al. [23] and Nabila et al. [24]; where they synthesized copper oxide nanoparticles and they evaluated their antibacterial activity against *Escherichia coli* and *Staphylococcus aureus* bacteria. They found that their materials exhibited antibacterial activity with maximum inhibition zones of 11 mm and 19 mm against *Escherichia coli* and *Staphylococcus aureus* bacteria, respectively. This finding is consistent with that of Mishra et al. [26] who reported the study of the effect of calcination temperature (400,600, and 800 °C) on the antibacterial activity of Cu–Zn-LDHs. They found that the Cu–Zn-LDHs samples calcined at 800 °C give better results compared to other materials calcined at 400 and 600 °C, and that uncalcined and calcined

samples are active up to 0.1 g/l, 0.05 g/l, respectively, of the copper content in LDHs which in agreement with our study. An observation of Tables 3 and 4 suggests that the bacterial inhibition capacity of calcined samples is more than those of uncalcined ones. This difference may be explained by the ejection of copper ions from the surface of this material, which was impossible in the uncalcined case due to the strongly bonded of copper with hydroxyl in layered double hydroxide, and to the effect of calcination on the particle size, resulting in smaller particle size and high surface area [17] because of the migration of Al^{3+} cation from octahedral sites to the tetrahedral position after calcination which increase the antibacterial activity of these materials. This result is in agreement with Huang et al. [45] who reported that the antibacterial activity of calcined LDHs increases by decreasing particle size and increasing the specific surface area due to the higher number of hydroxyl and superoxide (O_2^-) anions in solution. Also, these results are probably linked to the increase of the percentage of copper with the increase of calcination temperature; because after calcination, the material loses adsorbed water molecules which lead the formation of copper oxides resulting in better antibacterial activity.

Conclusion

A successful synthesis of efficient Cu-LDHs nanocomposites with different Cu/Al molar ratios has been developed using a simple co-precipitation method. The effect of calcination on the structural properties of Cu-LDHs was also studied. On the basis of XRD, all Cu-LDHs molar ratios Cu/Al are successfully synthesized and the best structure is attributed to $Cu_{0.05}$–$Al_{0.15}$-LDHs.

After calcination, the hydrotalcite structure is destroyed and leads to the formation of Cu and Mg oxides due to the dehydroxylation and decomposition of carbonate in the interlayer spacing. Based on the N_2-sorption–desorption results, the Cu-substituted LDHs had a macroporous structure with specific surface areas ranging between 98 m^2/g and 42 m^2/g. The uncalcined and calcined Cu-LDHs nanocomposites exhibited good antibacterial activity against both gram-negative (*Escherichia coli*, *Pseudomonas aeruginosa*) and gram-positive (*Staphylococcus aureus*, *Bacillus subtilis*, *Enterococcus faecalis*) bacteria. The calcined samples showed better antibacterial activity for all the Cu/Al molar ratios. Therefore, both uncalcined and calcined Cu-LDHs could be effective antibacterial materials used for various fields.

References

1. L. Jiang, Y. Binghuo, W. Kemei, J. Rare Earths **26**, 352–356 (2008)
2. K. Bakon, S. Palmer, R. Frost, J. Therm. Anal. Calorim. **100**, 125–131 (2010)
3. D.S. Tong, C.H.C. Zhou, M.Y. Li, W.H. Yu, J. Beltramini, C.X. Lin, Z.P.G. Xu, Appl. Clay Sci. **48**, 569–574 (2010)
4. T. Yamaoka, M. Abe, M. Tsuji, Mater. Res. Bull. **24**, 1183–1199 (1989)
5. A. Alejandre, F. Medina, P. Salagre, X. Correig, J. Sueiras, Chem. Mater. **11**, 939–948 (1999)
6. A.M. Fogg, G.R. Williams, R. Chester, D. O'Hare, J. Mater. Chem. **14**, 2369–2371 (2004)
7. G. Carja, R. Nakamura, T. Aida, H. Niiyama, Microporous Mesoporous Mater. **47**, 275–284 (2001)
8. Y. Kuang, L. Zhao, S. Zhang, F. Zhang, M. Dong, S. Xu, Materials **3**, 5220–5235 (2010)
9. M. Othman, Z. Helwani, W. Fernando, Appl. Organomet. Chem. **23**, 335–346 (2009)
10. H.-W. Olfs, L. Torres-Dorante, R. Eckelt, H. Kosslick, Appl. Clay Sci. **43**, 459–464 (2009)
11. J.J. Bravo-Suárez, E.A. Páez-Mozo, S.T. Oyama, Quim. Nova **27**, 574–581 (2004)
12. P. Benito, M. Herrero, F. Labajos, V. Rives, Appl. Clay Sci. **48**, 218–227 (2010)
13. P. Benito, M. Herrero, C. Barriga, F. Labajos, V. Rives, Inorg. Chem. **47**, 5453–5463 (2008)
14. H. Shi, J. He, J. Catal. **279**, 155–162 (2011)
15. A. Chakraborty, D.A. Islam, H. Acharya, Mater. Res. Bull. **120**, 110592 (2019)
16. J. Zhang, S. Gao, G. Wang, X. Ma, S. Jiao, D. Sang, S. Liu, M. Mao, H. Fang, J. Wang, Eur. J. Inorg. Chem. **2019**, 2654–2660 (2019)
17. L. Zhang, F. Li, D.G. Evans, X. Duan, Mater. Chem. Phys. **87**, 402–410 (2004)
18. H. Wang, Q. Gong, H. Huang, T. Gao, Z. Yuan, G. Zhou, Mater. Res. Bull. **107**, 397–406 (2018)
19. K. Parida, L. Mohapatra, N. Baliarsingh, J. Phys. Chem. C **116**, 22417–22424 (2012)
20. N. Baliarsingh, K. Parida, G. Pradhan, Ind. Eng. Chem. Res. **53**, 3834–3841 (2014)
21. A.K. Chatterjee, R. Chakraborty, T. Basu, Nanotechnology **25**, 135101 (2014)
22. J. Ramyadevi, K. Jeyasubramanian, A. Marikani, G. Rajakumar, A.A. Rahuman, Mater. Lett. **71**, 114–116 (2012)
23. S. Jadhav, S. Gaikwad, M. Nimse, A. Rajbhoj, J. Cluster Sci. **22**, 121–129 (2011)
24. M.I. Nabila, K. Kannabiran, Biocatal. Agric. Biotechnol. **15**, 56–62 (2018)
25. A. Ananth, S. Dharaneedharan, M.-S. Heo, Y.S. Mok, Chem. Eng. J. **262**, 179–188 (2015)
26. G. Mishra, B. Dash, S. Pandey, D. Sethi, Appl. Clay Sci. **165**, 214–222 (2018)

27. M. Zahraoui, A. Mokhtar, M. Adjdir, F. Bennabi, R. Khaled, A. Djelad, A. Bengueddach, M. Sassi, Res. Chem. Intermed. **45**, 633–644 (2019)
28. S. Brunauer, P.H. Emmett, J. Am. Chem. Soc. **59**, 2682–2689 (1937)
29. R. Allmann, H. Lohse, N. Jahrb, Mineral. Mh **6**, 161–181 (1966)
30. Y. Lwin, M.A. Yarmo, Z. Yaakob, A.B. Mohamad, W.R.W. Daud, Mater. Res. Bull. **36**, 193–198 (2001)
31. W.T. Reichle, Solid State Ionics **22**, 135–141 (1986)
32. M. Aramendia, Y. Avile, J. Mater. Chem. **9**, 1603 (1999)
33. A. Monshi, M.R. Foroughi, M.R. Monshi, World J. Nano Sci. Eng. **2**, 154–160 (2012)
34. R.D. Shannon, Acta Crystallogr. Sect. A Crystal Phys. Diffr. Theor. Gen. Crystallogr. **32**, 751–767 (1976)
35. J. RodríguezRuiz, A. PájaroPayares, E. MezaFuentes, Revista Colombiana de Química **45**, 33–38 (2016)
36. S. Britto, P.V. Kamath, J. Solid State Chem. **182**, 1193–1199 (2009)
37. K.S. Sing, Pure Appl. Chem. **57**, 603–619 (1985)
38. J. Broekhoff, J. De Boer, J. Catal. **9**, 8–14 (1967)
39. G. Mishra, B. Dash, S. Pandey, P.P. Mohanty, J. Environ. Chem. Eng. **1**, 1124–1130 (2013)
40. G. Mishra, B. Dash, D. Sethi, S. Pandey, B. Mishra, Environ. Eng. Sci. **34**, 516–527 (2017)
41. A. Mokhtar, A. Djelad, A. Boudia, M. Sassi, A. Bengueddach, J. Porous Mater. **24**, 1627–1636 (2017)
42. N. Bouchikhi, M. Adjdir, K.C. Bendeddouche, D. Bouazza, A. Mokhtar, F. Bennabi, H.A. Tabti, A. Sehmi, H. Miloudi, Mater Res Express **6**, 1250–1257 (2020)
43. M. Rivera-Garza, M. Olguın, I. Garcıa-Sosa, D. Alcántara, G. Rodrıguez-Fuentes, Microporous Mesoporous Mater. **39**, 431–444 (2000)
44. S.Z. Tan, K.H. Zhang, L.L. Zhang, Y.S. Xie, Y.L. Liu, Chin. J. Chem. **26**, 865–869 (2008)
45. L. Huang, D.-Q. Li, D. Evans, X. Duan, Eur. Phys. J. D At. Mol. Opt. Plasma Phys. **34**, 321–323 (2005)

Affiliations

Hadja Alia Tabti[1] · Mehdi Adjdir[2,3] · Abdelkader Ammam[4] · Baghdad Mdjahed[5] · Brahim Guezzen[5] · Amina Ramdani[6] · Choukry Kamel Benddedouche[7] · Noria Bouchikhi[1] · Nadir Chami[8]

[1] Laboratory of Physico-Chemical Studies, University Dr. Moulay Tahar, Saida, 20000 Saida, Algeria

[2] Departement of Engineering Process, Faculty of Technology, University Dr. Moulay Tahar, Saida, 20000 Saida, Algeria

[3] Institute of Functional Interfaces Section, Karlsruhe Institute of Technology (KIT), 76344 Eggenstein-Leopoldshafen, Karlsruhe, Germany

[4] Biotoxicology Pharmacognosy and Biological Valorization of Plants Laboratory, Department of Biology, Faculty of Science, University of Saïda Dr. Tahar Moulay, 20000 Saida, Algeria

[5] Laboratory of Separation and Purification Technology, Department of Chemistry, Faculty of Science, University of Tlemcen, Tlemcen, Algeria

[6] Laboratory of Materials and Catalysis, Faculty of Sciences, Site I BP 89 Djillali Liabès's University, 22000 Sidi Bel-Abbès, Algeria

[7] Laboratory of Applied Organic Synthesis, Faculty of Exact and Applied Sciences, University

Oran1 Ahmed Ben Bella, PO Box 1524, El M'Naouer, 31000 Oran, Algeria

[8] Department of Electronics, Faculty of Technology, University of Saïda Dr. Tahar Moulay, 20000 Saida, Algeria